

Invited research papers

Landscape evolution in the Liangzhu area since the early Holocene: A comprehensive sedimentological approach



Guangjiu Ling^a, Chunmei Ma^b, Qing Yang^{c,*}, Zhujun Hu^{a,d,**}, Hongbo Zheng^{c,e}, Bin Liu^f, Ningyuan Wang^f, Minghui Chen^f, Ye Zhao^f

^a School of Geography Science, Nanjing Normal University, Nanjing 210023, China

^b School of Geography and Ocean Science, Nanjing University, Nanjing 210023, China

^c Yunnan Key Laboratory of Earth System Science, Yunnan University, Kunming 650500, China

^d Jiangsu Center for Collaborative Innovation in Geographical Information Resource Development and Application, Nanjing Normal University, Nanjing 210023, China

^e School of Earth and Environmental Sciences, The University of Queensland, Brisbane, QLD 4072, Australia

^f Prehistoric Department, Zhejiang Provincial Institute of Cultural Relics and Archaeology, 310014 Hangzhou, China

ARTICLE INFO

Keywords:

Neolithic
Overbank flooding
Ca
Diatoms
Geomorphic evolution

ABSTRACT

The Liangzhu culture (5300–4300 cal yr BP) is considered to be the testification of the five thousand year history of Chinese civilization, and has thus attracted a great deal of attention from the archaeological community. However, the rise and fall of the Liangzhu culture, especially the cause of its vanishing, is still a topic of intense debate. Since the Liangzhu Ancient City area is a low-lying littoral region with a dense network of waterways, the landscape evolution would have had great impact on human-environment interactions. In this study, we will reconstruct the evolutionary history of the landscape by using sedimentological approach. Five sediment cores, together with trenches exposed in the archaeological sites were investigated. The chronology of the sediments was established by using twelve accelerator mass spectrometry (AMS) ¹⁴C dates. Sedimentary proxies, including calcium content, grain size, diatoms, and dinoflagellates are used for paleoenvironmental reconstruction. The results showed that: (1) from the last deglaciation to the early Holocene (before ca. 9400 cal yr BP), the Liangzhu area was widely exposed, and the cores contain coarse sand, gravel, and hard clay layers; (2) during the early to middle Holocene (ca. 9400 – 7600 cal yr BP), the area was rapidly submerged by a westward marine transgression, and the subsequent marine regression moved eastward from the Liangzhu area at approximately 7900 – 7600 cal yr BP when the rate of sediment supply exceeded the rate of relative sea level (RSL) rise; (3) during the middle to late Holocene (after ca. 7600 cal yr BP), the deposits mainly originated from overbank flooding or from storm surge events rather than from direct RSL rise from ca. 7600 – 6600 cal yr BP. The Liangzhu Ancient City area remained a swamp and an area of salinization until ca. 5100 cal yr BP.

1. Introduction

The Liangzhu culture is considered evidence of the five thousand years of Chinese civilization (Liu et al., 2018b) and is well known for its highly developed rice farming, jade objects associated with the burial of the Liangzhu elite and large-scale water engineering structures (Liu et al., 2017) (Fig. 1C, the high-dam, low-dam, and Tangshan levees). The archaeological ruins of Liangzhu City (approximately 5300–4300 cal yr BP) (Liu et al., 2017), located on the southwestern edge of the Yangtze Delta (Fig. 1B), were listed on the UNESCO World Heritage register in

2019. When the Liangzhu culture collapsed, the regional culture was replaced by a much less developed culture known as the Qianshangyang/Guangfulin/Maqiao culture (Chen et al., 1997; Chen, 2005; Zong et al., 2012) at approximately 4300 cal yr BP. Whether this collapse occurred due to environmental changes or to societal reasons has received much attention and remains a matter of debate.

At Neolithic sites in delta and low-lying regions, landscape changes under the influence of sea level change are a key driving factor for the spatial and temporal distribution of Neolithic sites during the early to middle Holocene (Wenke, 1991; Stanley and Warne, 1994, 1997;

* Correspondence to: Q. Yang, Yunnan Key Laboratory of Earth System Science, Yunnan University, Kunming 650500, China.

** Correspondence to: Z. Hu, School of Geography Science, Nanjing Normal University, Nanjing 210023, China.

E-mail addresses: chunmeima@nju.edu.cn (C. Ma), yangqing@ynu.edu.cn (Q. Yang), huzhujun86@163.com (Z. Hu), zhenghb@ynu.edu.cn (H. Zheng).

Funabiki et al., 2012; Liu et al., 2018a; Zheng et al., 2018). The detailed evolutionary processes of regional landscape development are vital for understanding the appearance and evolution of the Liangzhu culture. The Liangzhu area, as a low-lying littoral region on the northern shore of Hangzhou Bay, is highly vulnerable to even minor changes in sea level and to extreme climatic and environmental events, such as typhoons, storms, flooding, and saltwater intrusion (PAGES, 2009; Nicholls and Cazenave, 2010; Kirwan and Megonigal, 2013; Fan et al., 2017). Such environmental changes threaten human settlements and may have had critical impacts on Neolithic cultures. Previous studies have argued variously that the collapse of the Liangzhu culture may be ascribed to catastrophic environmental events, such as flash flooding (Zhu et al.,

1996; Zhang et al., 2004, 2005; Liu and Chen, 2012; Zong et al., 2012; Long et al., 2014; Wang et al., 2018), marine transgression (Stanley et al., 1999; Chen et al., 2008), and rapid climatic cooling (Innes et al., 2014; Li et al., 2018; Zhang et al., 2020). However, evidence for a rapid termination of the Liangzhu culture is scant. Some studies have explored the transgression and regression history of the Yangtze Delta (Chen and Stanley, 1998; Wang et al., 2012, 2013; Liu et al., 2015; He et al., 2018). Others have discussed the environmental conditions of the Liangzhu area during the Liangzhu culture (Li et al., 2010; Shi et al., 2011; Wang et al., 2017). However, systematic investigations of the detailed geomorphic evolution in the Liangzhu area during the Holocene are scarce. This hinders a comprehensive understanding of the relationship

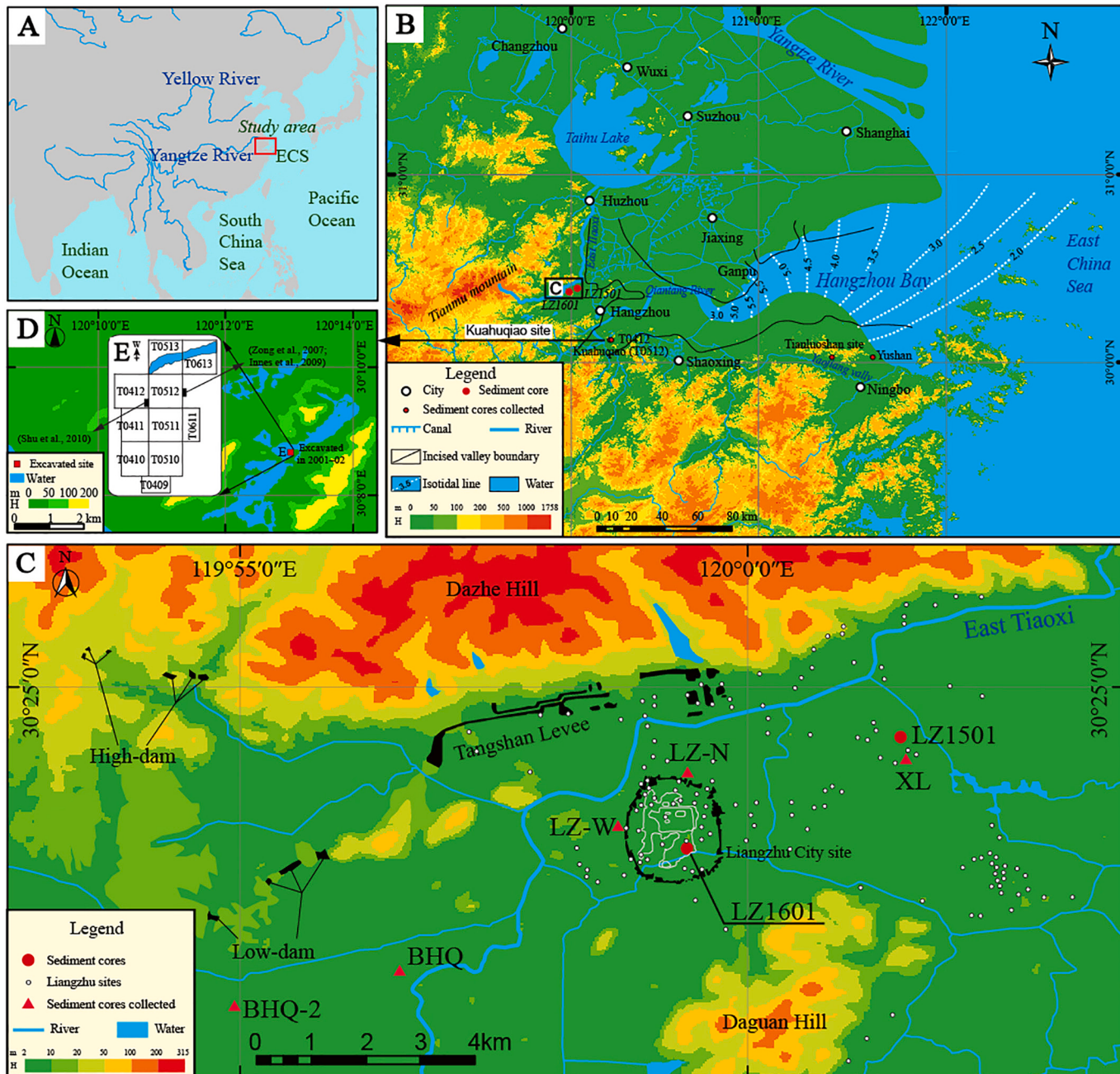


Fig. 1. Location map. A) Location of the study area in the lower reaches of the Yangtze River. (ECS = East China Sea). B) Yangtze Delta and the location of cores LZ1501 and LZ1601, the incised valley boundary line at ca. 7500 yr BP (Lin et al., 2005) and isotidal lines at present (Zhang et al., 2014). C) Topographic map showing the location of the Liangzhu City and the 5100-year-old hydraulic enterprise system (Liu et al., 2014), the sediment cores LZ1501, LZ1601, BHQ-2 (Jin, 2014), BHQ (Li, 2011), and XL (Liu et al., 2015), LZ-N (Wang et al., 2017), LZ-W (Wang et al., 2017), and the sites of Liangzhu culture (Luo, 2017). D) Locations of trenches T0412 (Shu et al., 2010) and T0512 (Zong et al., 2007; Innes et al., 2009) from Kuahuqiao site.

between the development of the Liangzhu culture and environmental changes in the Liangzhu area.

In this study, two cores (LZ1601 and LZ1501) were retrieved from the central area of the Liangzhu culture (the Liangzhu City area), and natural sedimentary exposures nearby that cover the time period from *ca.* 9400 to 4200 cal yr BP (Fig. 1C and 3) were examined. The sedimentary sequences were analyzed based on stratigraphy, sedimentology, chronology, and geo-archaeology. We generated a high-resolution, well-dated multiproxy data set including lithofacies, calcium (Ca) and strontium (Sr) abundances, grain size distribution, and diatom and dinoflagellate assemblages and compared these data to other regional proxies from previously published records (see Fig. 1B–E). The landscape evolution of the Liangzhu area since the early Holocene was therefore studied in detail, and the results include a history of the sea level changes, investigation of the geomorphic evolution and assessment of human adaptations in coastal China.

2. Geomorphic and climatic setting

The Hangzhou-Jiaxing-Huzhou Plain (Hangjiahu Plain) is situated in the southern portion of the Yangtze Delta, with the Qiantang River (QR) to the south and the Tianmu Mountains to the west (Fig. 1B). The Liangzhu City study area is located between Dazhe Hill and Daguan Hill, south of the Dongtiaoxi River, and borders a few low hills on the western and southwestern edges of the Hangjiahu Plain. The elevation is approximately 3 m above mean sea level (msl), and there is a dense waterway network (Fig. 1B and C). It is approximately 80 km from the Hangzhou Bay Bell Mouth (QR estuary) and approximately 200 km from the East China Sea. The present-day QR estuary is macrotidal in character, with a mean tidal range of 6.23–6.46 m during spring tides and 3.52–4.20 m during neap tides (Yang et al., 2002). The mean tidal range increases in a landward direction (Fig. 1C) as the tides (semidiurnal) propagate inland due to the rapid decrease in estuarine width and water depth (Fan et al., 2012). The maximum tidal range reaches 8.93 m near Ganpu, causing the formation of tidal bores (Fan et al., 2012) (see locations in Fig. 1B). The Dongtiaoxi River originates in the Tianmu Mountains and is the most influential river in this area. The river flows between Liangzhu City and the earthen dike system, flows northeast along the northern side of the Tianmu Mountains, and then terminates at Taihu Lake (Fig. 1B and C).

The climate of the study area is controlled by the Southeast Asian monsoon. According to instrumental records (1951–2013 CE at the Hangzhou Meteorological Station), the present mean annual precipitation is approximately 1400 mm, mainly from spring rains, the Meiyu front, and typhoon rains (Lu et al., 2015). The maximum daily precipitation is no less than 200 mm during the Meiyu period and approximately 400 mm during the typhoon rains in the eastern area of the Tianmu Mountains (Ren, 1995).

3. Materials and methods

Core LZ1501 ($30^{\circ}24'27.8''N$, $120^{\circ}2'3''E$) is 30.38 m long and was taken from ~4 km to the east of Liangzhu City in May 2015 (Fig. 1C). Core LZ1601 ($30^{\circ}23'29.7''N$, $119^{\circ}59'28.5''E$) is 21.10 m long and was taken approximately 1 km south of the Mojiaoshan palatial compound in Zhongjiagang inside Liangzhu City in May 2016 (Fig. 1C). The elevations of both cores were acquired by a real-time kinematic (RTK) measuring system (Model: TOPCON, HiPer SR) based on the 1985 Yellow Sea Datum (YSD). The elevations of cores LZ1501 and LZ1601 were 2.46 m and 0.82 m above the present msl YSD, respectively. Cores had a diameter of 88 mm, performed by a professional and scientific drilling company, with a more than 95% recovery rate.

3.1. Depositional facies and stratigraphic correlation

The lithologic and lithofacies characteristics of the sediment are

critical for understanding the relief and strata in the delta (e.g., Ta et al., 2002; Zhang et al., 2014; Liu et al., 2018a). We performed a detailed analysis of the lithology and lithofacies of the LZ1501 and LZ1601 cores and compared them with the sedimentary facies/lithology of some regional cores (BHQ-2, BHQ, and XL) and profiles (Trenches T0512 and T0412). The multiproxy data from the BHQ-2, BHQ, and XL cores around Liangzhu area and the Kuahuqiao T0512 and T0412 profiles are used for regional comparison. The proxies, including dating, lithology, mean grain size, CaO, diatom, foraminifera, and dinoflagellate contents, were obtained from previous results (Zong et al., 2007; Innes et al., 2009; Shu et al., 2010; Li, 2011; Jin, 2014; Liu et al., 2015; Ye et al., 2015, 2017; Cheng and Ye, 2019). BHQ-2 and BHQ are from the southwest of the Liangzhu City site, while XL is from the east of Liangzhu City (Fig. 1C). The trenches T0412 and T0512 of Kuahuqiao site are located the southeast of Liangzhu City site (Fig. 1D and E). The cores (BHQ-2, BHQ, LZ1601, LZ1501, and XL) form a transverse transect across the Liangzhu area and are used to reconstruct the paleoenvironmental history of the area during the Holocene.

3.2. Chronology

The chronology of the cores was developed using twelve accelerator mass spectrometry (AMS) ^{14}C dates (Fig. 2, Table 1). The AMS ^{14}C measurements were performed on plant materials (PM), wood, and organic matter (OM) by Beta Analytic Inc., Florida. The plant materials were pretreated by washing in NaOH and HCl, reduced to neutral pH and then converted to graphite. The AMS ^{14}C dates were converted into calendar years using Calib810 software (<http://calib.org/calib/calib.html>) and the INTCAL 20 and Marine 20 datasets (Heaton et al., 2020; Reimer et al., 2020) and are presented with 95% confidence intervals (2 σ) in years before the present (cal yr BP).

3.3. Abundance of elements

The relative concentrations of 28 elements were determined (as counts per second, cps) at 0.01 m intervals with an XRF core scanner (GEOTEK, MSCL-S). Each zone was scanned twice: once at 0.2 millamps (mA) and 10 kV to measure magnesium to rhodium (including Ca) and a second time at 0.8 mA and 40 kV to measure arsenic to lead (including Sr). A $15 \times 10\text{-mm}^2$ area of the core surface was irradiated with X-rays using a 20 s count time. We used Origin 2017 software with a 5-point (pts) fast Fourier transform filter (FFT) to reduce measurement noise.

3.4. Grain size distribution

Samples above the hard clay layer in LZ1501 and the gravel layer in LZ1601 were taken at 10 cm intervals for grain size analysis. Pretreatment was carried out by standard procedures (Lu and An, 1998). The grain size distribution was determined by the laser diffraction method using a Malvern Mastersizer-2000. The standard for an objective description of sediment was based on the Udden-Wentworth grain size scale.

3.5. Diatoms

A total of 18 and 13 samples were taken for diatom identification from cores LZ1501 and LZ1601, respectively. The 31 samples were selected from the representative lithology types in the two cores (Fig. 3). Five grams of dry sediment from each sample was treated with 30% H_2O_2 and 10% HCl at 60 °C to remove organic matter and carbonates, respectively. A 2.3 g/ml zinc bromide solution was applied for heavy liquid flotation. The sample residues were dried on a slide and permanently mounted in a neutral mounting medium. The diatoms were identified and counted under oil immersion at 1000 \times using an OLYMPUS BX-51 microscope until at least 300 valves were counted per sample. The taxonomic classification mainly followed Krammer and

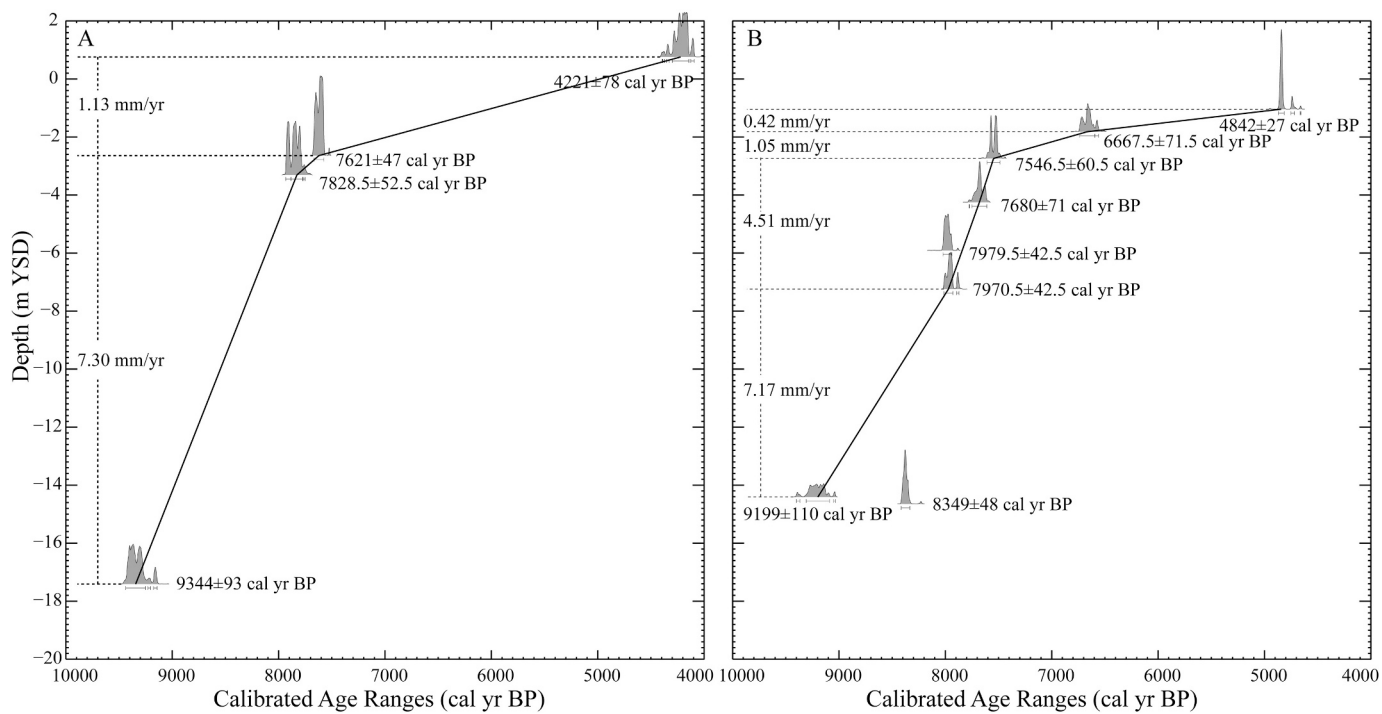


Fig. 2. Age-depth models for cores LZ1501 (A) and LZ1601 (B).

Table 1
AMS ^{14}C radiocarbon dates of material from the Liangzhu area.

Cores	Lab code	Depth (m YSD)	materials	Conventional Age (cal yr BP)	$\Delta\delta$ range (95%) (cal yr BP)	Sources
LZ1501	Beta527487	0.76	OM	3820 ± 30	4299– 4143	This study
	Beta415334	-2.64	PM	6760 ± 30	7668– 7574	
	Beta415335	-3.31	PM	7010 ± 30	7881– 7776	
	Beta415336	-17.41	PM	8310 ± 30	9437– 9251	
LZ1601	Beta459688	-1.04	Wood	4260 ± 30	4869– 4815	This study
	Beta523939	-1.82	OM	5840 ± 30	6739– 6596	
	Beta459690	-2.74	PM	6680 ± 30	7607– 7486	
	Beta459691	-4.25	Wood	6850 ± 30	7751– 7609	
	Beta459692	-5.91	PM	7170 ± 30	8022– 7973	
	Beta459693	-7.24	Wood	7130 ± 30	8013– 7928	
	Beta459694	-14.40	PM	8240 ± 30	9309– 9089	
BHQ	Beta459695	-14.46	PM	7520 ± 30	8396– 8301	Cheng and Ye (2019)
	Beta403431	-1.55	OM	5280 ± 30	6122– 5988	
	Beta403432	-3.5	OM	8860 ± 40	10,171– 9876	
	BA10482	-4.5	Peat	7095 ± 35	7979– 7841	
	BA10483	-4.6	Peat	7170 ± 70	8061– 7916	
	Beta403433	-6.92	OM	10,270 ± 40	12,106– 11,820	
	Beta360526	-8.42	Peat	7520 ± 40	8402– 8285	
BHQ – 2	BA10484	-15.05	Peat	9570 ± 90	11,185– 10,657	Zhang (2017)
	Beta403435	3.03	OM	380 ± 30	503– 425	
	Beta403434	1.98	OM	2210 ± 30	2326– 2144	
	Beta342637	0.28	CB	4200 ± 30	4762– 4687	
	Beta342638	-0.02	CB	3980 ± 30	4525– 4403	
	Beta358869	-4.65	Wood	7085 ± 40	7979– 733	
	Beta342635	-13.77	Shell	7780 ± 40	8609– 8447	
XL	Beta342636	-14.22	Shell	7990 ± 40	9000– 8716	Liu et al. (2015)
	Beta288643	-3.4	Plant	6640 ± 40	7577– 7461	
	Beta288644	-5.1	Plant	6600 ± 40	7519– 7428	
	Beta288645	-19.38	Shell	8330 ± 40	8904– 8490	
	Beta288646	-21.26	Shell	8350 ± 40	8931– 8527	
	Beta288647	-21.76	Shell	8280 ± 40	8810– 8417	
	Beta288648	-22.25	Shell	8320 ± 40	8889– 8474	
	Beta288649	-22.55	Shell	8430 ± 40	8994– 8620	
	Beta288650	-22.68	Shell	8450 ± 40	9010– 8634	
	Beta288651	-22.8	Shell	8460 ± 40	9020– 8639	

OM = Organic matter; PM = plant materials; CB = Calcium binding. The bold text (**Beta459692**, **Beta459695**, **Beta403432**, **Beta403433**, and **Beta342638**) indicates reversed data.

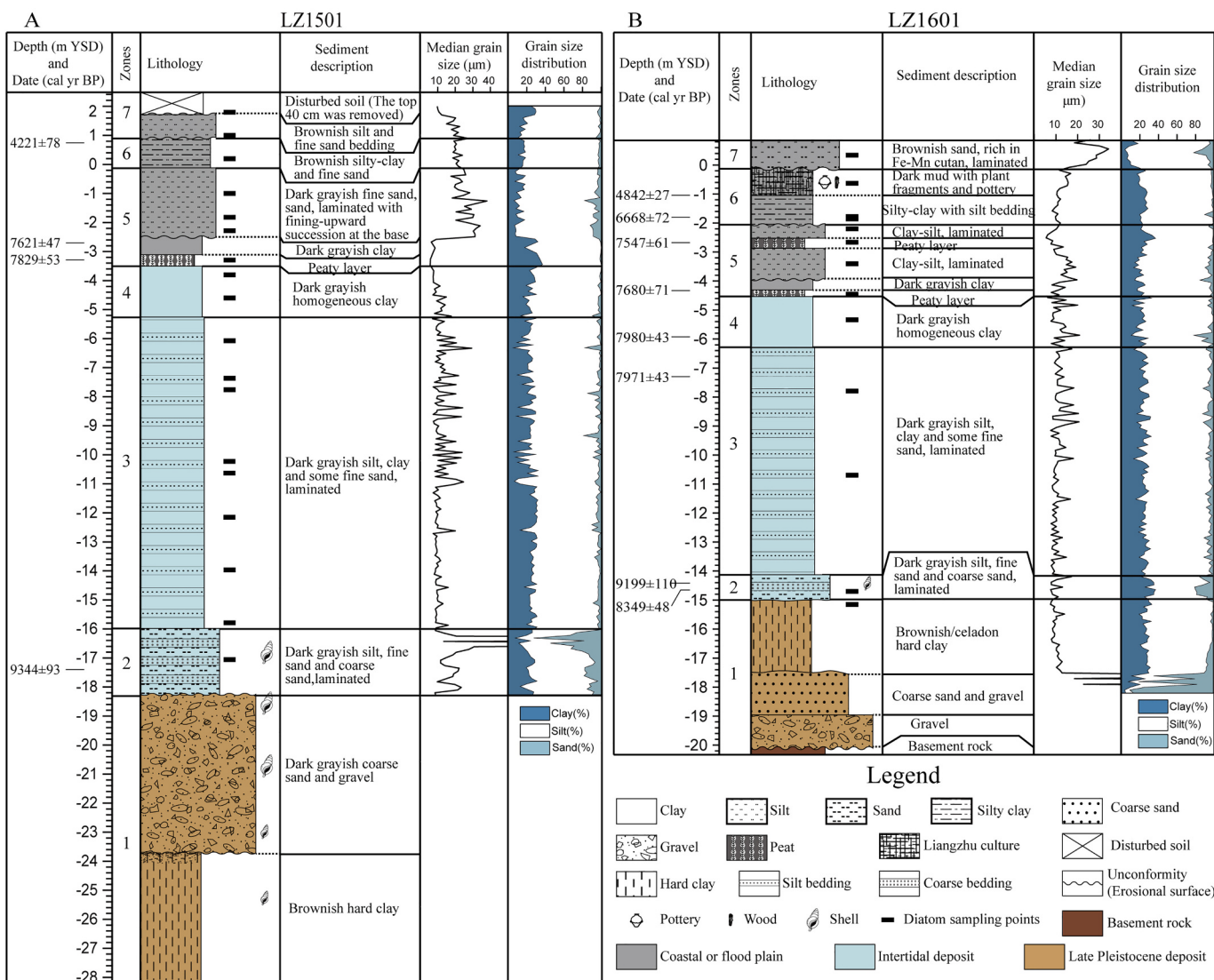


Fig. 3. Lithology, radiocarbon ages, sediment description, grain size distribution, and photographs of cores LZ1501 and LZ1601.

Lange-Bertalot (2012), Guo and Qian (2003) and Jin et al. (1992).

3.6. Dinoflagellates

In total, 127 samples were collected for dinoflagellate cyst identification from core LZ1501. The standard hydrofluoric acid method was performed (Faegri et al., 1989). Lycopodium spores ($27,560 \pm 563$ grains/tablet) were added to the samples to estimate the dinoflagellate cyst concentrations. The sample residues were identified and counted at $400\times$ using an OLYMPUS BX-51 microscope.

3.7. Holocene Sea level curve records

Holocene sea level data were obtained from work published elsewhere. The global sea level curve was obtained from Lambeck et al. (2014). The curves of the relative sea level (RSL) curve for the Yangtze Delta were obtained from Zong (2004), Liu et al. (2015, 2018a) and Sun et al. (2019).

3.8. Tectonic subsidence and sedimentary compaction

Due to the slow subsidence effect in the Yangtze Delta Plain (Hu et al., 1993) and possible sedimentary compaction, the elevations of the

upper part of zone 5 in LZ1501 (elevation and range: $-2.48 \sim -0.15$ m) and LZ1601 (elevation and range: $-3.96 \sim -2.11$ m) were corrected. We adopted a subsidence rate of 0.100 ± 0.023 m/kyr, as suggested by Xiong et al. (2018), to correct for the tectonic subsidence. The sedimentary compaction was estimated to be 10% of the initial thickness of the compressible sequence(s) beneath the dated horizon divided by the post depositional elapsed time as a proportion of the past 9000 years (Xiong et al., 2018).

4. Results

4.1. Radiocarbon chronology

The twelve AMS ^{14}C dates from cores LZ1601 and LZ1501 are provided in Table 1. The calculated ages of cores LZ1601 and LZ1501 range from ca. 9400 cal yr BP to ca. 4200 cal yr BP. The dates from core LZ1601 at -14.46 m and -14.40 m (Beta 459,695 and Beta 459,694) were reversed. The date at -14.40 m (9309–9089 cal yr BP) was more reliable based on a comparison with the lithology and the age of core LZ1501. Two other dates from core LZ1601 at -5.91 m and -7.24 m were also reversed. The later date was chosen because the wood is often considered more reliable as a dating material. Based on the AMS ^{14}C dates, the LZ1601 and LZ1501 cores showed a rapid sedimentation rate

from ca. 9400–7600 cal yr BP (4.51–7.30 mm/yr, average of 6.33 mm/yr), while the sedimentation rate significantly decreased thereafter (0.42–1.13 mm/yr, average of 0.80 mm/yr) (Fig. 2). Additionally, twenty-three AMS ^{14}C dating results from cores BHQ (Cheng and Ye, 2019), BHQ-2 (Zhang, 2017), and XL (Liu et al., 2015) are shown in Table 1.

4.2. Lithology and sedimentary facies

Based on detailed lithological descriptions, grain size distributions, sediment structures, and fossil remains, cores LZ1501 and LZ1601 can be divided into seven zones (Fig. 3); see details below. Photographs of cores LZ1501 and LZ1601 are shown in Fig. 4.

Zone 1, from the bottom, is brownish hard clay from $-28.32 \sim -23.77$ m and coarse sand/gravel from $-23.77 \sim -18.21$ m with occasional occurrences of some shell debris in core LZ1501. Core LZ1601 contains bedrock at the bottom, which is overlain by brownish gravel and coarse sand from $-20.14 \sim -17.54$ m and brownish to greenish hard layers from $-17.54 \sim -14.99$ m.

Zone 2 is dark grayish sand and coarse sand with laminated layers (LZ1501: $-18.21 \sim -15.97$ m; LZ1601: $-14.99 \sim -14.12$ m), with abundant shell debris and plant fragments.

Zone 3 is dark grayish silty clay and silt with parallel bedding layers (LZ1501: $-15.97 \sim -5.24$ m; LZ1601: $-14.12 \sim -6.26$ m), and the bedding exhibits typical fining-upward and thinning-upward successions at the top of each layer.

Zone 4 is characterized by a homogeneous dark grayish clay layer (LZ1501: $-5.24 \sim -3.53$ m; LZ1601: $-6.26 \sim -4.52$ m).

Zone 5, from the bottom, includes a peaty layer from $-3.53 \sim -3.13$ m, dark grayish homogeneous clay from $-3.13 \sim -2.54$ m, and dark grayish silt with fine sandy beds from $-2.54 \sim -0.15$ m (see Fig. 4, twisted or contorted) in core LZ1501. Core LZ1601 contains a peaty layer from $-4.52 \sim -4.27$ m, dark grayish homogeneous clay from $-4.27 \sim -3.96$ m, dark grayish silt with fine sandy beds from $-3.96 \sim -2.86$ m (see Fig. 4, twisted or contorted), a peaty layer from $-2.86 \sim -2.47$ m and a silty clay layer with thin silt beds from $-2.47 \sim -2.11$ m.

There is an unconformity (erosional surface, located at approximately -2.54 m in core LZ1501 and approximately -3.96 m in core LZ1601) between the clay and sandy beds.

In zone 6, dark grayish clayey silt interbedded with a few subtle sand laminae (-0.15 – 0.86 m) is observed in core LZ1501, and brownish oxidation begins to appear and increases significantly from the bottom to the top. Core LZ1601 contains dark grayish silty clay at -2.11 – -1.04 m, which is overlain by a culture layer at -1.04 – -0.12 m. There are fine sandy beds followed by typical fining-upward and thinning-upward successions at the base of the silty clay layer. An unconformity surface appears at approximately -2.11 m in core LZ1601.

Zone 7 is brownish silt interbedded with fine sand layers (LZ1501: 0.86–1.76 m; LZ1601: -0.12–0.82 m) and disturbed soil (1.76–2.46 m in core LZ1501). Parallel bedding is common, with typical fining-upward and thinning-upward successions in the brownish silt layer interbedded with fine sand layers. There is an erosional surface at its base (located at approximately 0.86 m in core LZ1501 and approximately -0.12 m in core LZ1601). Top samples of the two cores were not collected because of human disturbance.

4.3. Abundance of elements

Calcium (Ca) is often used as an indicator of marine sedimentation (e.g., Arz et al., 2001; Van Rooij et al., 2006; Yao, 2016). The synchronous changes in Ca and strontium (Sr) indicate that the sources of Ca are mainly marine biogenic minerals (Carlson et al., 2008; Hodell et al., 2008). Here, we present only the Ca and Sr data from the XRF scanning (Fig. 5) and carry out the Pearson correlation analysis for the two elements at different periods.

In zone 1 in core LZ1501, Ca is stable at low levels, while the Sr level fluctuates widely. In zones 2–5, Ca and Sr are synchronous ($R = 0.84$, $p < 0.01$). In zones 6–7, the two elements show synchronous changes ($R = 0.63$, $p < 0.01$), but the amplitude of the changes in Ca is greater than that in Sr.

In core LZ1601, the content of Ca shows low values, and the Sr presents great fluctuation in zone 1. In zones 2– 5, Ca and Sr are

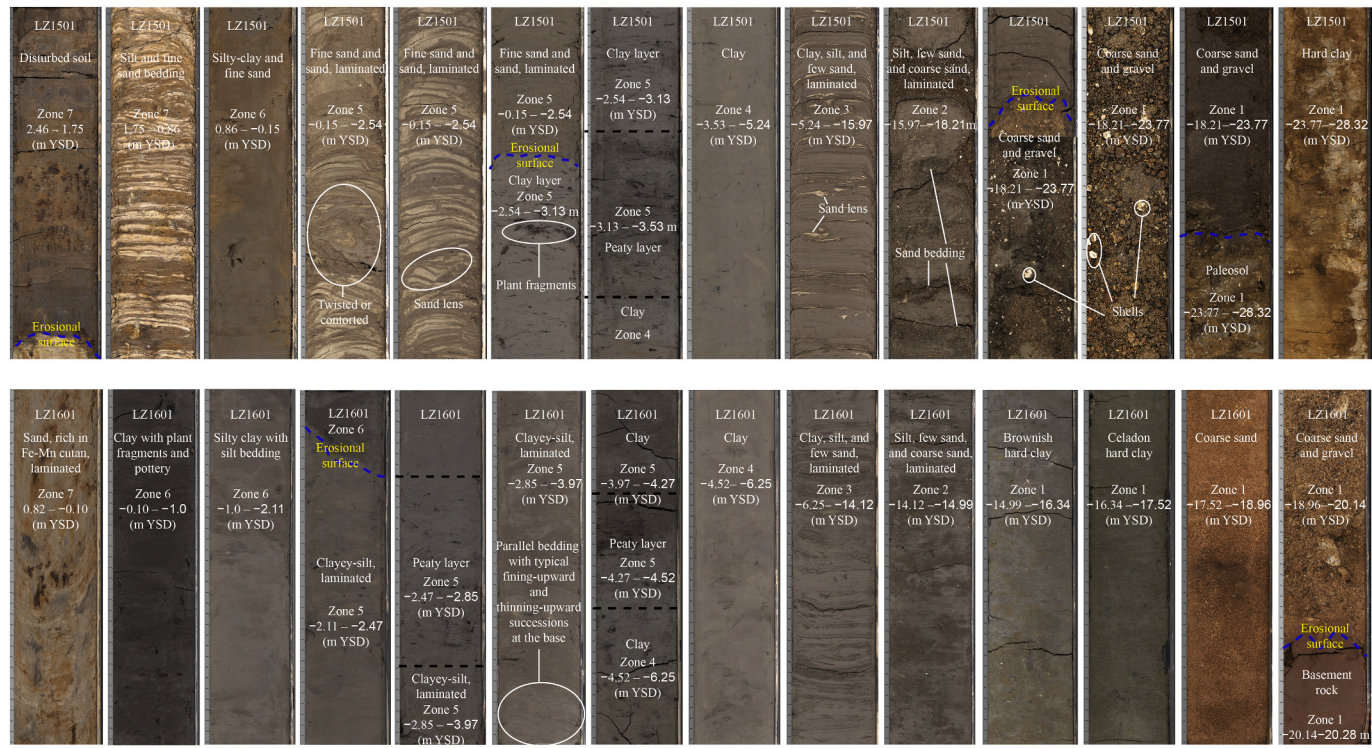


Fig. 4. Photographs of cores LZ1501 and LZ1601.

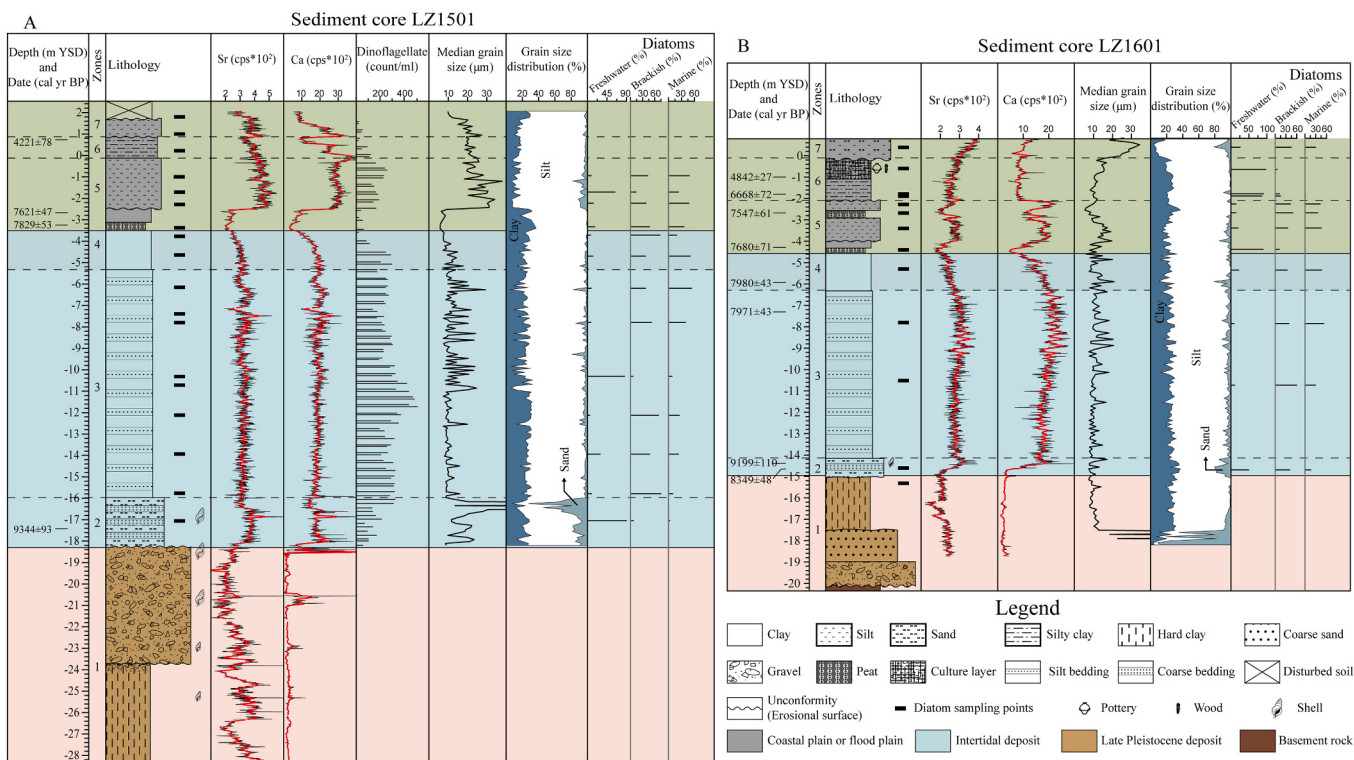


Fig. 5. Sediment lithology, chronology, Ca, Sr, median grain size, grain size distribution, and diatoms of cores LZ1501 and LZ1601. The red lines for Ca and Sr are 5 pts. FFT smooth. (For interpretation of the references to colour in this figure legend, the reader is referred to the web version of this article.)

synchronous ($R = 0.74$, $p < 0.01$). In zone 6, Ca returns to a low level, but Sr shows high abundance, with a weaker correlation between the two elements ($R = 0.20$, $p < 0.01$). In zone 7, the abundances of Ca and Sr increase slightly ($R = 0.54$, $p < 0.01$).

4.4. Diatom analysis

Diatoms can be classified and plotted as freshwater, brackish, and marine forms (Figs. 5 and 6). The freshwater diatom assemblages in the

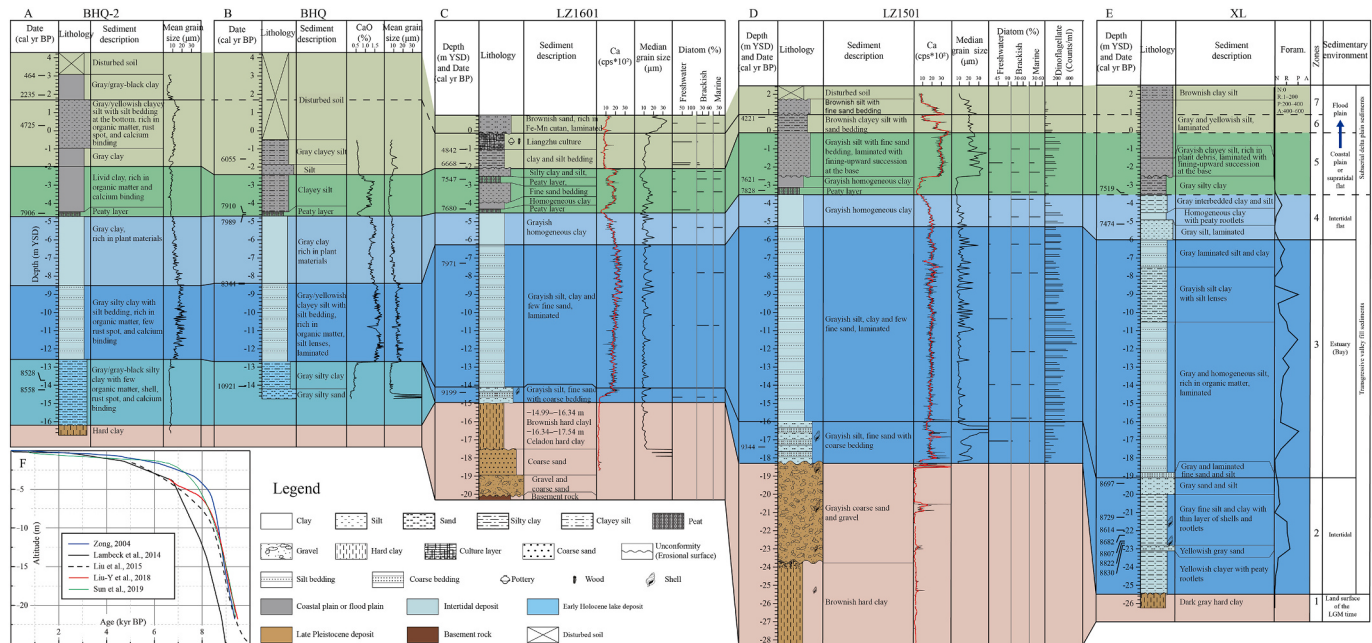


Fig. 6. A ~ E) Comprehensive comparison of multiple indicators from cores BHQ-2 (Jin, 2014; Zhang, 2017), BHQ (Li, 2011; Ye et al., 2015; Ye et al., 2017; Cheng and Ye, 2019), LZ1601, LZ1501, and XL (Liu et al., 2015). Elevation, lithology, and chronology are shown for all 5 cores; mean grain size is shown for cores BHQ-2 and BHQ; CaO is shown for core BHQ; Ca, median grain size, and diatoms are shown for cores LZ1601 and LZ1501; dinoflagellates are shown for core LZ1501; and foraminifera are shown for core XL. F) The Holocene global curve (Lambeck et al., 2014) and the RSL curves in the Yangtze Delta (Zong, 2004; Lambeck et al., 2014; Liu et al., 2015; Liu et al., 2018a; Sun et al., 2019). The red line for Ca is 5 pts. FFT smooth. (For interpretation of the references to colour in this figure legend, the reader is referred to the web version of this article.)

cores were dominated by *Achnanthes minutissima* and *Aulacoseira* spp.; the brackish diatom assemblages were dominated by *Cyclotella stylorum*, *Diploneis smithii*, and *Melosira sulcata* var. *sulcata*; and the marine diatom assemblages were dominated by *Actinocyclus ehrenbergii*, *Actinoptychus undulatus*, *Actinoptychus splendens*, and *Arcocellulus cornucervis*. The detailed results we obtained are as follows.

In core LZ1501, there is a very low concentration of diatoms in zone 1. Freshwater types dominate the diatom assemblages in zone 2. In zones 3–5, the diatom groups are primarily marine and brackish. The abundance of diatoms at –10.78 m and –7.37 m are much lower than the statistical standard (300 valves), and any interpretation is therefore unreliable; this is also true for zones 6–7.

In zone 1 in core LZ1601 (–17.54 ~ –14.99 m, hard clay), there is also a low concentration of diatoms. The diatom assemblages in zone 2 are dominated by freshwater types. In zones 3–5, the major diatoms are marine and brackish forms, except in one sample (–4.40 m, the peaty layer). The diatoms at –4.40 m are primarily freshwater groups. In zone 6, freshwater diatoms (91.51% on average) dominated by *Aulacoseira* spp. and *Navicula* spp. are the assemblage's major components. In zone 7, freshwater, brackish and marine diatoms are all common types and are represented by *Navicula* spp., *Diploneis suborbicularis*, and *M. sulcata* and *A. cornucervis*, respectively.

4.5. Dinoflagellate analysis

The dinoflagellate analyses for core LZ1501 are shown in Fig. 5A. The samples contained abundant dinoflagellate, in which *Spiniferites* spp. dominated. Dinoflagellates are an essential indicator of the impact of seawater environments (Cho and Matsuoka, 2001). In zone 1, the dinoflagellate concentration is low, with 3.36 grains/ml on average. The dinoflagellate concentration shows an increasing trend to 160.37 grains/ml on average in zone 2. In zone 3, dinoflagellate concentrations rise to peak levels, with 277.05 grains/ml on average. The dinoflagellate concentration declines to 174.71 grains/ml on average in zone 4. In zone 5, the dinoflagellate concentration is low in the lower part (–3.53 ~ –2.54 m), with 43.01 grains/ml on average, and is high in the upper part (–2.54 ~ –0.15 m), with 182.08 grains/ml on average. The dinoflagellate concentration declines to 67.71 grains/ml on average in zone 6. In zone 7, the dinoflagellate concentration is also low, with 22.97 grains/ml on average.

5. Discussion

5.1. Geomorphological evolution of the Liangzhu area

The lithology, lithofacies, and multiproxy data from the LZ1501 and LZ1601 cores correlated with previously published literature in the study region reveal the detailed geomorphological process in the Liangzhu area since the late Pleistocene (Fig. 6). The late Pleistocene-Holocene strata are grouped into zone 1: late Pleistocene hard clay sediments; zones 2–4: early to middle Holocene transgressive sequence; and zones 5–7: mid-late Holocene subaerial delta plain sediments (Fig. 7).

5.1.1. Late Pleistocene terrestrial deposits (zone 1, until ca. 9400 cal yr BP)

Except in core BHQ, zone 1 sediments consist of slightly oxidized hard clay, yellowish-grayish coarse sand, and gravel with burial depths ranging from –15.0 m to –18.3 m below the present sea level (Figs. 5 and 6). Previous studies have suggested that hard clay is widely distributed in the Yangtze Delta, Hangjiahu, and Ningbo-Shaoxing (Ningshao) plains and represents basal relief during the Last Glacial Maximum (LGM), with burial depths ranging from a few meters to several tens of meters (Chen and Stanley, 1998; Li et al., 2000; Qin et al., 2008). Based on the stratigraphic correlation, the age of the first hard clay layer (the hard clay in zone 1) has been assigned to the end of the late Pleistocene in the Yangtze River Delta (Qin et al., 2008). AMS ^{14}C

dating showed that it formed during the period of 25,000–12,000 yr BP (Ming and Wang, 1979; Li et al., 1986; Sun and Wu, 1987; Cai et al., 2001). The basal section of core LZ1601 includes coarse sand and gravel below the hard clay (Fig. 3B and 6C), which may be indicative of late Pleistocene or earlier fluvial sedimentation at the base of the Liangzhu valley (Lin et al., 2005). The basal section of core LZ1501 contains gravel deposits above the hard clay (Fig. 3A and 6D), which may represent late Pleistocene or early Holocene consolidated deposits of colluvial and alluvial origin (Fig. 7A1 and A2).

5.1.2. Early to middle Holocene transgressive dynamics (zones 2–4, ca. 9400–7900 cal yr BP)

In zone 2, the sediments in both LZ1501 and LZ1601 are composed of silt, fine and coarse sand with laminated layers and were deposited during ca. 9400–9200 cal yr BP. The Ca contents of both cores and the dinoflagellate content of LZ1501 show an increasing-upward pattern and an abundance of brackish-marine diatom species (Fig. 6C and D). These characteristics indicate an intertidal environment during a marine transgression. The intertidal area was quickly submerged by a rapid RSL rise (average of approximately 15 mm/yr from 9500 to 8000 yr BP) (Fig. 6F), and the intertidal area migrated to the west from ca. 9400 to 9200 cal yr BP, as shown by the sediment facies of cores LZ1501 and LZ1601 (Figs. 6 and 7). The concentration of foraminifera in zone 2 in core XL shows an increasing trend (Fig. 6E) (Liu et al., 2015), reflecting the increased influence of seawater during this stage. In contrast, a freshwater lake or swamp conditions are inferred for the base of cores BHQ-2 and BHQ in the early Holocene period (Lu and Ye, 2014), indicating that the seawater did not reach BHQ-2 and BHQ until approximately 8500 cal yr BP.

In zone 3, the sediments at the LZ1501, LZ1601, BHQ, BHQ-2, and XL sites consist of clay and silty clay with silt beds. The Ca content at the LZ1501, LZ1601, and BHQ sites, the concentration of foraminifera at the XL site, and the dinoflagellate content of LZ1501 all show high values. These features reveal an estuary or bay environment with marine influence. The high sedimentation accumulation rate of more than 7.30 mm/yr in cores LZ1501 and LZ1601 signified a rapid infilling period (Fig. 2).

The sediment facies in zone 4 at the LZ1501, LZ1601, BHQ, BHQ-2, and XL sites are characterized by a high clay content with plant materials and peaty rootlets. The Ca content (LZ1501, LZ1601, and BHQ), dinoflagellate content (LZ1501), and abundance of foraminifera (XL) show decreasing-upward trends. This evidence indicates that the marine influence decreased at ca. 7900 cal yr BP, forming an intertidal flat environment. On the eastern coast of China, the Yangtze Delta began to form at ca. 8000 cal yr BP, and the sea level was relatively stable at that time (Hori and Saito, 2007; Wang et al., 2010). On the Ningshao Plain (Fig. 1B), southeast of the Liangzhu area, the RSL reached its maximum flooding surface at ca. 7900 cal yr BP and then remained stable from ca. 7900–7600 cal yr BP (Liu et al., 2018a). Freshwater marshes and lagoons gradually replaced estuarine depositional environments during this period at the Kuahuqiao site (Innes et al., 2009).

5.1.3. Mid-late Holocene subaerial delta plain sediments (zones 5–7, ca. 7900 cal yr BP to present)

The mid-late Holocene subaerial delta plain sediments in cores LZ1501 and LZ1601 can be divided into two parts: a coastal plain and a flood plain (Fig. 6C and D, zones 5–7). The appearance of the salt marsh peat layer at the base of zone 5 in cores BHQ, BHQ-2, LZ1501, and LZ1601 indicates the initiation of a terrestrial environment (e.g., Gehrels, 1999; Horton et al., 2005; Bird et al., 2010; Wang et al., 2013) (Fig. 6). The peaty layers in zone 5 (Fig. 6B, C, and D) have low Ca values (BHQ, LZ1601, and LZ1501) and reduced dinoflagellate numbers, indicating the initiation of a freshwater environment (Cho and Matsuoka, 2001; Yao, 2016). The sediments in zone 5 are devoid of foraminifera in XL and reflect the formation of a terrestrial landscape (Fig. 6E) (Liu et al., 2015). The peaty layer sediments at the base of zone

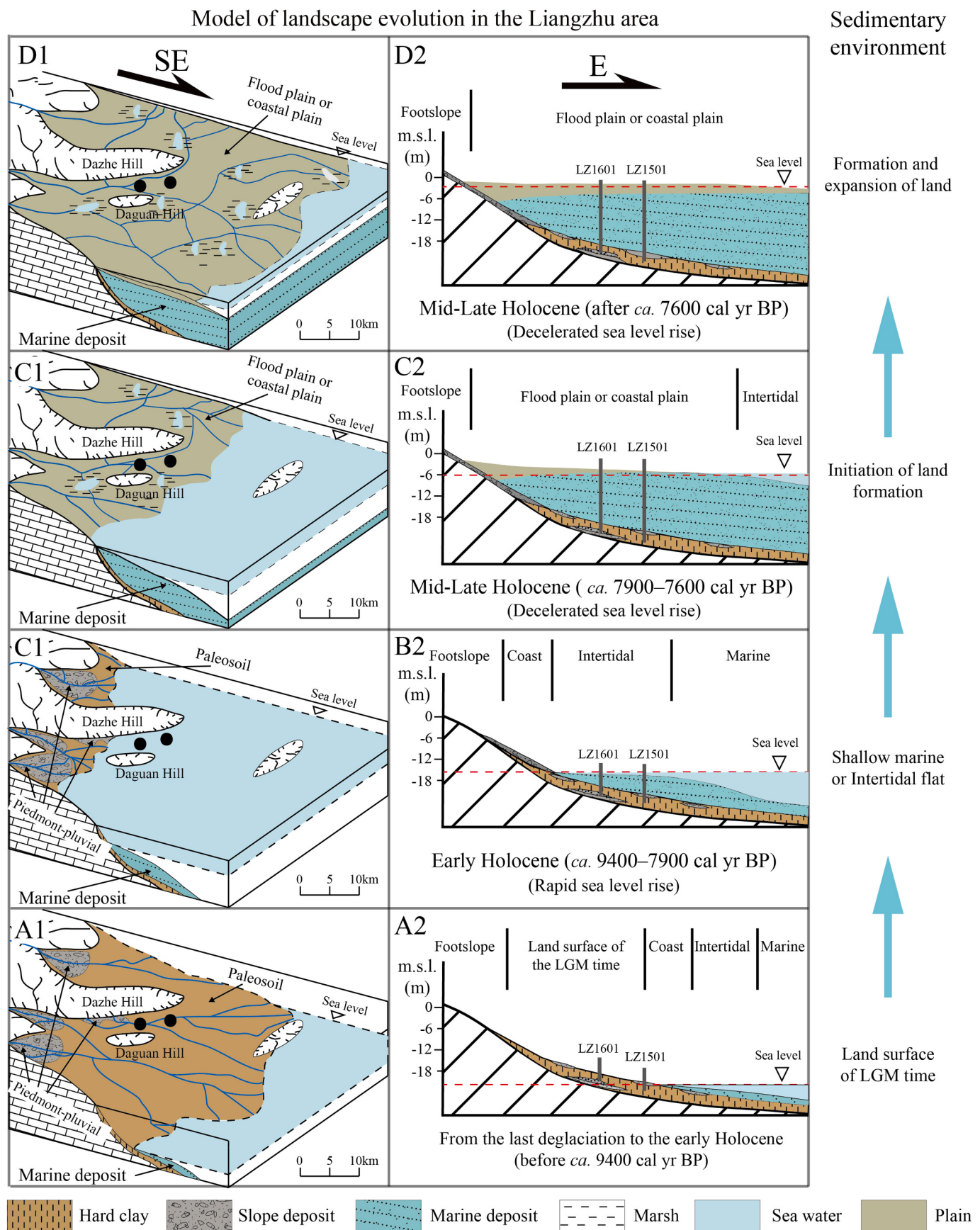


Fig. 7. Sketch maps of the landscape changes in the Liangzhu area since the Holocene based on the analysis of cores BHQ-2, BHQ, LZ1601, LZ1501, and XL.

5 were dated to 7906 cal yr BP (BHQ-2), 7989–7910 cal yr BP (BHQ), 7680 cal yr BP (LZ1601), and 7828 cal yr BP (LZ1501). Therefore, it can be inferred that terrestrial conditions in the Liangzhu area occurred during *ca.* 7900–7600 cal yr BP. This timing is consistent with the marine regression period of *ca.* 7900–7600 cal yr BP in the Yaojiang Valley (Dai et al., 2018), and the lower-salinity settings prevailing after 7500 cal yr BP on the Dongtiaoxi River Plain (Chen et al., 2018).

An unconformity contact (erosional surface) between the upper and lower parts of zone 5 occurs in cores LZ1601 (*ca.* –3.96 m), LZ1501 (*ca.* –2.54 m), and XL (*ca.* –2.50 m). The upper part displays a fining-upward succession consisting of grayish silt, fine sand beds (twisted or contorted), and a peaty layer deposited during *ca.* 7600–6600 cal yr BP (Fig. 4 and 5). These features suggest deposition under turbulent conditions (Ta et al., 2002; Davis Jr., 2012). The diatom assemblages in the upper part of zone 5 in LZ1601 and LZ1501 are dominated by brackish and marine taxa (Fig. 6C and D, zone 5), and the associated sediments

feature high Ca contents and high dinoflagellate concentrations, indicating a marine influence between *ca.* 7600 and 6600 cal yr BP (Cho and Matsuoka, 2001; Yao, 2016; Zong et al., 2013) (see more detail in Section 5.2). Additionally, the high content of Ca in equivalent sediments in BHQ (Ye et al., 2017) also indicates seawater intrusion (Fig. 6B, zone 5).

The flood plain deposits (zones 6–7) show two different conditions according to the lithology changes in cores LZ1601 and LZ1501 (Fig. 6C and D). An erosional surface separates the upper (zone 7) and lower (zone 6) parts in cores LZ1601 and LZ1501. The presence of freshwater diatom species (LZ1601), low Ca values (LZ1501 and LZ1601), and low dinoflagellate concentrations (LZ1501) reflects an increasing freshwater influence at approximately 6600–4200 cal yr BP (Fig. 6C and D). The low Ca content in zone 6 in core BHQ also indicates a freshwater environmental setting at approximately 6100 cal yr BP (Ye et al., 2017) (Fig. 6B). In zone 7, there are fining-upward and thinning-upward successions at its base in LZ1501, reflecting a flooding event deposit at *ca.*

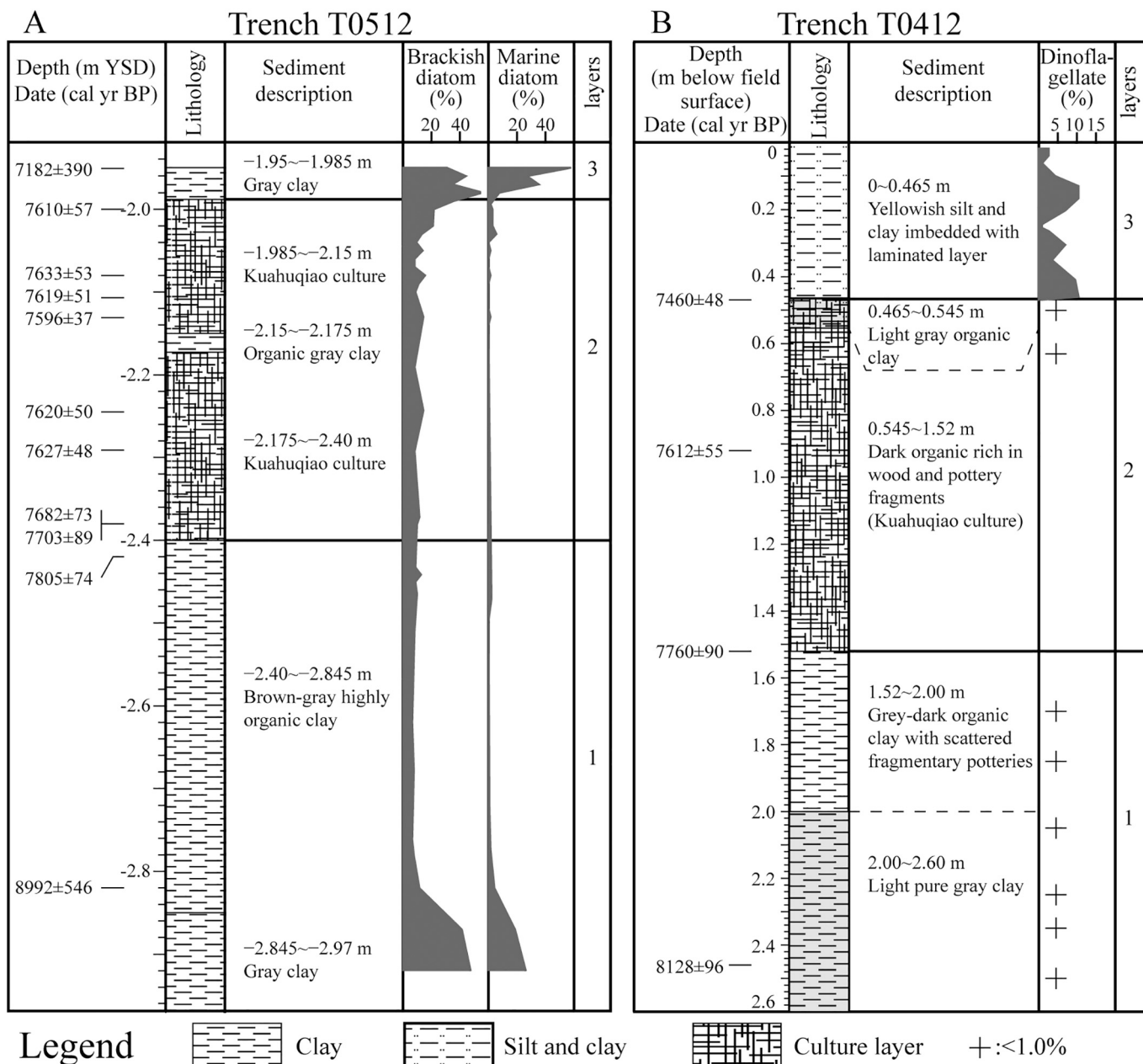


Fig. 8. Lithology, chronology, diatom and dinoflagellate of two profiles of the Kuahuqiao site: A) T0512 (Zong et al., 2007; Innes et al., 2009); B) T0412 (Shu et al., 2010).

4200 cal yr BP in the Liangzhu City area. Furthermore, this zone in LZ1601 contains an abundance of marine and brackish diatom species, and the high Ca values at the base in LZ1501 indicate that the event was associated with saltwater intrusion.

5.2. The saltwater deposits between ca. 7600 and 6600 cal yr BP

The saltwater sedimentary process during approximately 7600–6600 cal yr BP did not occur only in the Liangzhu area. Similar deposits that formed at almost the same time (approximately 7400 cal yr BP) have been observed at Kuahuqiao, located to the southeast of Liangzhu and separated by the QR (Fig. 1B, D, and E). Laminated silt and clay and high abundances of marine/brackish diatoms and dinoflagellate cysts have been found above the Kuahuqiao cultural layer (Fig. 8, layer 3) (Innes et al., 2009; Shu et al., 2010). The facies show yellowish silt and clay with laminated layers cutting into the Kuahuqiao culture layer (Zhejiang Provincial Institute of Cultural Relics and Archaeology Xiaoshan Museum, 2004), suggesting a powerful hydrodynamic influence during an accretionary phase (Ta et al., 2002; Davis Jr, 2012). This deposit is different from a typical intertidal flat or estuarine deposit containing homogeneous clay (Innes et al., 2009; Shu et al., 2010) (Fig. 8, layer 1).

Previous studies have proposed that the saltwater sedimentation can be attributed to direct inundation and increasingly saline conditions (Zong et al., 2007; Innes et al., 2009; Shu et al., 2010; Liu et al., 2015). This inference arose partially from the uncertainty concerning the nature and rate of sea level changes in eastern coastal China during the Holocene. This uncertainty has led to the persistence of two basically opposing models: either the sea level rose to levels higher than the present-day YSD from approximately 7500–6600 cal yr BP before falling to its current level (Li et al., 2014; Xiong et al., 2020), or alternatively, the sea level has risen continuously from the early Holocene to the present (Liu et al., 2018a; Sun et al., 2019). The reconstruction of global sea level history suggests that there has been no high sea level stands (i.e., higher than the current level) during the entire Holocene (Fig. 6F) (Lambeck et al., 2014). Previous sedimentological investigations have confirmed that the sea level history of eastern coastal China resembles that of the global reconstruction, with minor regional differences (Zheng et al., 2018). The Holocene global sea level curve (Lambeck et al., 2014) and the RSL curves for the Yangtze Delta (Zong, 2004; Liu et al., 2015; Liu et al., 2018a; Sun et al., 2019) suggest that the sea level was at approximately −5 m at ca. 7600 cal yr BP (Fig. 7F), which is below the elevation of the upper parts of zone 5 in LZ1501 (corrected elevation and range: −0.19–1.68 m) and LZ1601 (corrected elevation and range: −2.11–0.63 m) (Table 2) and layer 3 in Kuahuqiao (Fig. 8A, approximately −2.0 m) (Zong et al., 2007; Innes et al., 2009). Based on this, it can be inferred that the saltwater sedimentation in the upper part of zone 5 (cores LZ1501 and LZ1601) and layer 3 in Kuahuqiao was not caused by direct marine inundation. The strong hydrodynamic sedimentary evidence indicates that it was more likely an overbank flooding event or storm surge deposit.

Since 7500 cal yr BP, a wide coastal plain developed above the incised valley fill of the QR and the adjacent interfluvial sediments (Fig. 1B) (Lin et al., 2005). The ancient mouth of the QR was located

near Hangzhou at approximately 7500 cal yr BP (Fig. 1B, incised valley boundary) (Lin et al., 1999, 2005). The tidal amplitude may have increased from 1.6 m to 2.2 m at the head of Hangzhou Bay due to the paleotopographic change during the period 7.6–4.5 cal kyr BP, according to simulation results (Wang et al., 2020). Overbank flooding is currently closely associated with large tidal bores in the QR estuary, where the mean and maximum spring tidal ranges reach 6.44 m and 9.00 m, respectively (Fan et al., 2014; Zhang et al., 2014). Accordingly, combining the above sediment facies characteristics, the elevation comparison, and the tidal bores in Hangzhou Bay, it can be inferred that overbank flooding or storm surge deposits likely caused contemporaneous deposits in the upper part of zone 5 in the Liangzhu area (Fig. 6) and in layer 3 at Kuahuqiao (Fig. 8). This unit has not been described precisely or given a reasonable explanation but is of crucial archaeological significance.

5.3. Cultural response to geomorphological evolution and environmental change

A stable environment and food supply were often critical for Neolithic settlements (Stanley and Warne, 1997). Sea level changes have been the primary factor controlling landscape evolution in the coastal plain during the Holocene (Stanley and Warne, 1994; Zheng et al., 2018). The settling of land in the Yangtze Delta and Ningshao Plains area occurred before 7000 cal yr BP (Hori et al., 2001; Wang et al., 2010, 2012; Liu et al., 2018a), and Majiabang settlements and Hemudu settlements were widely distributed in these areas during ca. 7000–6000 cal yr BP (Zheng et al., 2009; Liu and Chen, 2012; Wang, 2019a). The Liangzhu City area is situated west of the Yangtze Delta (Fig. 1B), and the marine regression began much earlier at approximately 7900–7600 cal yr BP. However, the earliest Neolithic sites of the Liangzhu City area developed at approximately 5100 cal yr BP, at least 1000 years later than those in the Yangtze Delta and Ningshao Plains (Wang et al., 2012; Liu et al., 2018a; Zheng et al., 2018; Qin, 2019).

Sedimentary evidence indicates that the differential local landscape evolution process is the key factor resulting in the much later Neolithic development in the Liangzhu City area. As mentioned above (see Sections 5.1.3 and 5.2), the sedimentary environment was characterized by overbank flooding or a storm surge in the Liangzhu City area during approximately 7600–6600 cal yr BP, rendering the area unsuitable for Neolithic occupation. Then, it was controlled mainly by freshwater conditions with decreasing marine influence until 5100 cal yr BP (Shi et al., 2011). During this period, the East Asian summer monsoon was strengthened (Wang et al., 2005), which may have induced increased erosion in the drainage, and a vast amount of sediment may have been delivered to the lower reaches and the river mouth, forming a flood plain and a river delta. The Liangzhu area, a low-lying littoral region, was vulnerable to the increased threat of flooding from the western mountains (Fig. 1B and C). Accordingly, the Liangzhu City area may have been a swamp with some soil salinization accompanying flooding during approximately 6600–5100 cal yr BP (Liu et al., 2015; Shi et al., 2011).

After ca. 5100 cal yr BP, the RSL rise rate in eastern China decreased (Fig. 6F). The swamp environment in the Liangzhu City area then started to dry out as the coastal plain developed farther eastward (Shi et al.,

Table 2

Corrections for the postdepositional lowering of the upper parts of zone 5.

Core	Elevation and range (m YSD)	Compressible age of the base (cal yr BP)	Compressible age of the top (cal yr BP)	Compressible thickness and range (m YSD)	Total compaction and range (m) ^a	Tectonic subsidence and range (m) ^b	Corrected elevation and range (m YSD)
LZ1501	−2.48 ~ −0.15	~7600	~6650	18.06–15.73	1.53–1.16	0.76–0.67	−0.19–1.68
LZ1601	−3.96 ~ −2.11	~7600	~6650	12.88–11.03	1.09–0.81	0.76–0.67	−2.11–0.63

^a The sedimentary compaction was estimated to be 10% of the initial thickness of the compressible sequence(s) beneath the dated horizon divided by the post-depositional elapsed time proportional to the past 9000 years (Xiong et al., 2018).

^b An average subsidence rate of 0.100 ± 0.023 mm/a is applied for correction (Xiong et al., 2018).

2011). In addition, the 5100-year-old hydraulic enterprise system (Liu et al., 2017), including high dams, low dams, and the Tangshan levees at the basal slopes of the Tianmu Mountains (Fig. 1C), provided multiple functions, such as flood control, transportation, and irrigation (Wang, 2019b). These new lands in the Liangzhu City area (which provide fertile soil accumulation, a reliable fresh water supply, perennial aquatic food sources, ease of travel and trade, forests and hunting), protected by hills, were attractive for immigration and settlement expansion (Stanley and Warne, 1997).

6. Conclusions

Lithology and multiproxy analyses were carried out on two cores from the Liangzhu area covering the period from ca. 9400–4200 cal yr BP. The analyses were considered in combination with published analyses of other cores in this study area. The cores provide data on the processes of landscape development in the Liangzhu area since the early Holocene. The major findings are as follows:

- (1) From the last deglaciation to the early Holocene (before ca. 9400 cal yr BP), the Liangzhu area was an exposed surface, and coarse sands, gravels, and hard clay are present in the cores.
- (2) In the early to middle Holocene (ca. 9400–7600 cal yr BP), the Liangzhu area was rapidly submerged by a marine transgression from east to west at ca. 9400–7900 cal yr BP. Marine regression occurred eastward from the Liangzhu area at approximately 7900–7600 cal yr BP as the sediment supply rate exceeded the RSL rise rate during the period of deceleration in the rate of RSL change.
- (3) The mid-late Holocene (after ca. 7600 cal yr BP) deposits in zone 5 in the Liangzhu City area came from overbank flooding or storm surges rather than from direct marine inundation from ca. 7600–6600 cal yr BP. The Liangzhu City area remained a swamp with some salinization until ca. 5100 cal yr BP, when the Liangzhu City area became suitable for Neolithic settlement and agriculture.

Declaration of competing interest

No conflict of interest exists in the submission of this manuscript, and manuscript is approved by all authors for publication. We declare that we do not have any commercial or associative interest that represents a conflict of interest in connection with the work submitted. I would like to declare on behalf of my co-authors that the work was original research that has not been published previously, and not under consideration for publication elsewhere, in whole or in part. All the authors listed have approved the manuscript that is enclosed.

Acknowledgments

We thank Yousheng Zhou, Yingying Wang, and Yeting Cao for their assistance in field work. Dr. Xiaochun Wei, Dr. Zhi Zhang and Dr. Pon-nusamy Saravanan are appreciated for comments on an early draft of the manuscript. This work was supported by the National Natural Science Foundation of China (grant numbers 41772369, 41672344, and 41671196), the National Basic Research Program of China (grant number 2015CB953803), and the Yunnan Leading Talent Program (grant number 202005AB160008).

References

- Arz, H.W., Pätzold, J., Moammar, M.O., Röhl, U., 2001. Late Quaternary climate records from the Northern Red Sea: results on gravity cores retrieved during the R/V METEOR cruise M44/3. *J. King Abdul Aziz Univ. Mar. Sci.* 1 (12), 101–113. <https://doi.org/10.4197/mar.12-1.7>.
- Bird, M.I., Austin, W.E.N., Wurster, C.M., Fifield, L.K., Mojtabid, M., Sargeant, C., 2010. Punctuated eustatic sea-level rise in the early mid-Holocene. *Geology* 38 (9), 803–806. <https://doi.org/10.1130/G31066.1>.
- Cai, Y., Zhang, W., Guo, Z., Chen, Y., Chen, Z., 2001. Climate fluctuation of the Western Shanghai District by correspondence analysis since 8.5 ka B.P. *J. Lake Sci.* 2 (13), 118–126. <https://doi.org/10.18307/20010204> (in Chinese with English abstract).
- Carlson, A.E., Stoner, J.S., Donnelly, J.P., Hillaire-Marcel, C., 2008. Response of the southern Greenland Ice Sheet during the last two deglaciations. *Geology* 36 (5), 359–362. <https://doi.org/10.1130/G24519A.1>.
- Chen, J., 2005. Ecological history view on the rise and decline of Liangzhu culture. *South. Cult. (5)*, 33–40 (in Chinese with English abstract).
- Chen, Z., Stanley, D.J., 1998. Sea-level rise on Eastern China's Yangtze Delta. *J. Coast. Res.* 14 (1), 360–366.
- Chen, Z., Hong, X., Li, S., Wang, L., Shi, X., 1997. Study of archaeology-related environment evolution of Taihu Lake in southern Chang Jiang delta plain. *Acta Geograph. Sin.* 64 (2), 37–43 (in Chinese with English abstract).
- Chen, Z., Zong, Y., Wang, Z., Wang, H., Chen, J., 2008. Migration patterns of Neolithic settlements on the abandoned Yellow and Yangtze River deltas of China. *Quat. Res.* 70 (2), 301–314. <https://doi.org/10.1016/j.yqres.2008.03.011>.
- Chen, T., Ryves, D.B., Wang, Z., Lewis, J.P., Yu, X., 2018. Mid- to late Holocene geomorphological and hydrological changes in the south Taihu area of the Yangtze delta plain, China. *Paleogeogr. Paleoclimatol. Paleoceanol.* 498, 127–142. <https://doi.org/10.1016/j.palaeo.2018.03.012>.
- Cheng, L., Ye, W., 2019. Multi-proxy evidence for paleoclimate evolution performed on a paleolake sediment core in the East Asian Monsoon Region. *Environ. Earth Sci.* 78 (3), 92. <https://doi.org/10.1007/s12665-019-8107-5>.
- Cho, H., Matsuoka, K., 2001. Distribution of dinoflagellate cysts in surface sediments from the Yellow Sea and East China Sea. *Mar. Micropaleontol.* 42 (3), 103–123. [https://doi.org/10.1016/S0377-8398\(01\)00016-0](https://doi.org/10.1016/S0377-8398(01)00016-0).
- Dai, B., Liu, Y., Sun, Q., Ma, F., Chen, J., Chen, Z., 2018. Foraminiferal evidence for Holocene environmental transitions in the Yaojiang Valley, South Hangzhou Bay, eastern China, and its significance for Neolithic occupations. *Mar. Geol.* 404, 15–23. <https://doi.org/10.1016/j.margeo.2018.07.001>.
- Davis Jr., R.A., 2012. Tidal signatures and their preservation potential in stratigraphic sequences. In: Davis Jr., R.A., Dalrymple, R.W. (Eds.), *Principles of Tidal Sedimentology*. Springer, Dordrecht, pp. 33–35. https://doi.org/10.1007/978-94-007-0123-6_3.
- Faegri, K., Kaland, P.E., Krzywinski, K., 1989. *Textbook of Pollen Analysis*, 4 ed. John Wiley & Sons, Ltd, New York.
- Fan, D., Cai, G., Shang, S., Wu, Y., Zhang, Y., Gao, L., 2012. Sedimentation processes and sedimentary characteristics of tidal bores along the north bank of the Qiantang Estuary. *Chin. Sci. Bull.* 57 (13), 1578–1589. <https://doi.org/10.1007/s11434-012-4993-6>.
- Fan, D., Tu, J., Shang, S., Cai, G., 2014. Characteristics of tidal-bore deposits and facies associations in the Qiantang Estuary, China. *Mar. Geol.* 348, 1–14. <https://doi.org/10.1016/j.margeo.2013.11.012>.
- Fan, D., Wu, Y., Zhang, Y., Burr, G., Huo, M., Li, J., 2017. South Flank of the Yangtze Delta: past, present, and future. *Mar. Geol.* 392, 78–93. <https://doi.org/10.1016/j.margeo.2017.08.015>.
- Funabiki, A., Saito, Y., Phai, V., Nguyễn, H., Haruyama, S., 2012. Natural levees and human settlement in the Song Hong (Red River) delta, northern Vietnam. *The Holocene* 22 (6), 637–648. <https://doi.org/10.1177/0959683611430847>.
- Gehrels, W.R., 1999. Middle and Late Holocene sea-level changes in Eastern Maine reconstructed from foraminiferal saltmarsh stratigraphy and AMS ^{14}C dates on basal peat. *Quat. Res.* 52 (3), 350–359. <https://doi.org/10.1006/qres.1999.2076>.
- Guo, Y., Qian, S., 2003. *Flora Algarum Marinarum Sinicarum: Bacillariophyta, Centricae*. Science Press, Beijing, p. 493 (in Chinese).
- He, K., Lu, H., Zheng, Y., Zhang, J., Xu, D., Huang, X., Wang, J., Lei, S., 2018. Middle-Holocene Sea-level fluctuations interrupted the developing Hemudu culture in the lower Yangtze River, China. *Quat. Sci. Rev.* 188, 90–103. <https://doi.org/10.1016/j.quascirev.2018.03.034>.
- Heaton, T.J., Köhler, P., Butzin, M., Bard, E., Reimer, R.W., Austin, W.E.N., Ramsey, C.B., Grootes, P.M., Hughen, K.A., Kromer, B., Reimer, P.J., Adkins, J., Burke, A., Cook, M.S., Olsen, J., Skinner, L.C., 2020. Marine20—the marine radiocarbon age calibration curve (0–55,000 CAL BP). *Radiocarbon* 62 (4), 779–820. <https://doi.org/10.1017/RDC.2020.68>.
- Hodell, D.A., Channell, J.E.T., Curtis, J.H., Romero, O.E., Röhl, U., 2008. Onset of “Hudson Strait” Heinrich events in the eastern North Atlantic at the end of the middle Pleistocene transition (~640 ka)? *Paleoceanography* 23 (4), PA4218. <https://doi.org/10.1029/2008PA001591>.
- Hori, K., Saito, Y., 2007. An early Holocene Sea-level jump and delta initiation. *Geophys. Res. Lett.* 34 (18), L18401. <https://doi.org/10.1029/2007GL031029>.
- Hori, K., Saito, Y., Zhao, Q., Cheng, X., Wang, P., Sato, Y., Li, C., 2001. Sedimentary facies of the tide-dominated paleo-Changjiang (Yangtze) estuary during the last transgression. *Mar. Geol.* 177 (3), 331–351. [https://doi.org/10.1016/S0025-3227\(01\)00165-7](https://doi.org/10.1016/S0025-3227(01)00165-7).
- Horton, B.P., Gibbard, P.L., Milne, G.M., Morley, R.J., Purintavaragul, C., Stargardt, J.M., 2005. Holocene Sea levels and palaeoenvironments, Malay-Thai Peninsula, Southeast Asia. *The Holocene* 15 (8), 1199–1213. <https://doi.org/10.1191/0959683605hl891rp>.
- Hu, H., Huang, L., Yang, G., 1993. Recent vertical crustal deformation in the coastal area of eastern China. *Sci. Geol. Sin.* 28 (3), 270–278 (in Chinese with English abstract).
- Innes, J.B., Zong, Y., Chen, Z., Chen, C., Wang, Z., Wang, H., 2009. Environmental history, palaeoecology and human activity at the early Neolithic forager/cultivator site at Kuahuqiao, Hangzhou, eastern China. *Quat. Sci. Rev.* 28 (23), 2277–2294. <https://doi.org/10.1016/j.quascirev.2009.04.010>.
- Innes, J.B., Zong, Y., Wang, Z., Chen, Z., 2014. Climatic and palaeoecological changes during the mid- to Late Holocene transition in eastern China: high-resolution pollen

- and non-pollen palynomorph analysis at Pingwang, Yangtze coastal lowlands. *Quat. Sci. Rev.* 99, 164–175. <https://doi.org/10.1016/j.quascirev.2014.06.013>.
- Jin, L., 2014. The Environmental Records of BHQ-2 Core during Holocene in Pingyao (Master). Zhejiang Normal University, Jinhua, China (in Chinese with English abstract).
- Jin, D., Cheng, Z., Liu, S., 1992. Chinese Marine Benthic Diatoms, Vol. II. Ocean press, Beijing, p. 437 (in Chinese).
- Kirwan, M.L., Megonigal, J.P., 2013. Tidal wetland stability in the face of human impacts and sea-level rise. *Nature* 504, 53–60. <https://doi.org/10.1038/nature12856>.
- Krammer, K., Lange-Bertalot, H., 2012. European Diatom Identification System. Zhongshan University Press, Guangzhou, China, p. 493 (in Chinese).
- Lambeck, K., Rouby, H., Purcell, A., Sun, Y., Cambridge, M., 2014. Sea level and global ice volumes from the Last Glacial Maximum to the Holocene. *Proc. Natl. Acad. Sci. U. S. A.* 111 (43), 15296–15303. <https://doi.org/10.1073/pnas.1411762111>.
- Li, L., 2011. The Environment Change and Cultural Response in the Early Holocene in Zhejiang Province (Master). Zhejiang Normal University, Jinhua, China (in Chinese with English abstract).
- Li, C., Ming, Q., Sun, H., 1986. Holocene strata and transgressions at the Southern flank of the Yangtze Delta. *Chin. Sci. Bull.* (21), 1650–1653 (in Chinese).
- Li, C., Chen, Q., Zhang, J., Yang, S., Fan, D., 2000. Stratigraphy and paleoenvironmental changes in the Yangtze Delta during the Late Quaternary. *J. Asian Earth Sci.* 18 (4), 453–469. [https://doi.org/10.1016/S1367-9120\(99\)00078-4](https://doi.org/10.1016/S1367-9120(99)00078-4).
- Li, Y., Wu, J., Hou, S., Shi, C., Mo, D., Liu, B., Zhou, L., 2010. Palaeoecological records of environmental change and cultural development from the Liangzhu and Qujialing archaeological sites in the middle and lower reaches of the Yangtze River. *Quat. Int.* 227 (1), 29–37. doi:10.1016/j.quaint.2010.05.015.
- Li, G., Li, P., Liu, Y., Qiao, L., Ma, Y., Xu, J., Yang, Z., 2014. Sedimentary system response to the global sea level change in the East China Seas since the last glacial maximum. *Earth Sci. Rev.* 139, 390–405. <https://doi.org/10.1016/j.earscirev.2014.09.007>.
- Li, C., Li, Y., Zheng, Y., Yu, S., Tang, L., Li, B., Cui, Q., 2018. A high-resolution pollen record from East China reveals large climate variability near the Northgrippian-Meghalayan boundary (around 4200 years ago) exerted societal influence. *Paleogeogr. Paleoclimatol. Paleoecol.* 512, 156–165. <https://doi.org/10.1016/j.palaeo.2018.07.031>.
- Lin, C., Huang, Z., Zhu, S., Li, C., Jiang, W., 1999. Late quaternary sedimentary characteristics and processes in the Hangzhou Bay Coastal Plain. *Acta Geol. Sin.* 73 (2), 120–130 (in Chinese with English abstract).
- Lin, C., Zhuo, H., Gao, S., 2005. Sedimentary facies and evolution in the Qiantang River incised valley, eastern China. *Mar. Geol.* 219 (4), 235–259. <https://doi.org/10.1016/j.margeo.2005.06.009>.
- Liu, L., Chen, X., 2012. The Archaeology of China: From the Late Paleolithic to the Early Bronze Age. Cambridge University Press.
- Liu, B., Wang, N., Zheng, Y., Chen, X., Zhou, W., Yan, K., Chen, M., Qi, Z., Lu, X., Chen, Q., Xu, Y., Fan, C., 2014. Findings of archaeological survey of prehistoric city at Liangzhu during 2006–2013. *South. Cult.* 2, 31–38 (in Chinese with English abstract).
- Liu, Y., Sun, Q., Thomas, I., Zhang, L., Finlayson, B., Zhang, W., Chen, J., Chen, Z., 2015. Middle Holocene coastal environment and the rise of the Liangzhu City complex on the Yangtze delta, China. *Quat. Res.* 84 (3), 326–334. <https://doi.org/10.1016/j.yqres.2015.10.001>.
- Liu, B., Wang, N., Chen, M., Wu, X., Mo, D., Liu, J., Xu, S., Zhuang, Y., 2017. Earliest hydraulic enterprise in China, 5,100 years ago. *Proc. Natl. Acad. Sci. U. S. A.* 114 (52), 13637–13642. <https://doi.org/10.1073/pnas.1710516114>.
- Liu, Y., Sun, Q., Fan, D., Dai, B., Ma, F., Xu, L., Chen, J., Chen, Z., 2018a. Early to Middle Holocene Sea level fluctuation, coastal progradation and the Neolithic occupation in the Yaojiang Valley of southern Hangzhou Bay, Eastern China. *Quat. Sci. Rev.* 189, 91–104. <https://doi.org/10.1016/j.quascirev.2018.04.010>.
- Liu, B., Wang, N., Chen, M., 2018b. Liangzhu: The Earliest State Society in East Asia. China Social Sciences Network. http://www.cssn.cn/zx/bwyc/201809/t2018092_8_4636709.shtml?COLLC=3580668593& (in Chinese).
- Long, T., Qin, J., Atahan, P., Mooney, S., Taylor, D., 2014. Rising waters: New geoarchaeological evidence of inundation and early agriculture from former settlement sites on the southern Yangtze Delta, China. *The Holocene* 24 (5), 546–558. <https://doi.org/10.1177/0959683614522309>.
- Lu, H., An, Z., 1998. Paleoclimatic significance of grain size of loess-palaeosol deposit in Chinese Loess Plateau. *Sci. China Ser. D-Earth Sci.* 41 (6), 626–631. <https://doi.org/10.1007/BF02878745>.
- Lu, W., Ye, W., 2014. Characteristics of pollen assemblage and climate change in the Holocene at Borehole BHQ in Pingyao area, Zhejiang Province. *J. Palaeogeogr.* 16 (5), 687–701. <https://doi.org/10.7605/gdlxb.2014.05.55> (in Chinese with English abstract).
- Lu, X., Lu, B., Deng, S., 2015. Variation analysis and forecast of precipitation in Hangzhou over the past 63 years. *Water Power* 41 (11), 17–20 (in Chinese with English abstract).
- Luo, X., 2017. The archaeological exhibition can do so: the review of “Kingdom—special exhibition to commemorating the eight years of Liangzhu Archaeology”. *Pop. Archaeol.* 64–70 (in Chinese).
- Ming, Q., Wang, P., 1979. Quaternary transgressions in Shanghai region. *J. Tongji Univ.* (2), 109–128 (in Chinese with English abstract).
- Nicholls, R.J., Cazenave, A., 2010. Sea-level rise and its Impact on coastal zones. *Science* 328 (5985), 1517–1520. <https://doi.org/10.1126/science.1185782>.
- PAGES, 2009. Science Plan and Implementation Strategy. IGBP Secretariat, No. 57. Stockholm, 67 pp.
- Qin, L., 2019. The formation of Liangzhu Complex: a preliminary report of chronological study. In: A Comprehensive Study of Liangzhu Ancient City. Cultural Relics Press, Beijing, pp. 335–377 (in Chinese).
- Qin, J., Wu, G., Zheng, H., Zhou, Q., 2008. The palynology of the first Hard Clay Layer (late Pleistocene) from the Yangtze delta, China. *Rev. Palaeobot. Palynol.* 149 (1–2), 63–72. <https://doi.org/10.1016/j.revpalbo.2007.10.003>.
- Reimer, P.J., Austin, W.E.N., Bard, E., Bayliss, A., Blackwell, P.G., Ramsey, C.B., Butzin, M., Cheng, H., Edwards, R.L., Friedrich, M., Grootes, P.M., Guilderson, T.P., Hajdas, I., Heaton, T.J., Hogg, A.G., Hughen, K.A., Kromer, B., Manning, S.W., Muscheler, R., Palmer, J.G., Pearson, C., Plicht, J.V.D., Reimer, R.W., Richards, D.A., Scott, E.M., Southon, J.R., Turney, C.S.M., Wacker, L., Adolphi, F., Büntgen, U., Capano, M., Fahrni, S.M., Fogtmann-Schulz, A., Friedrich, R., Köhler, P., Kudsk, S., Miyake, F., Olsen, J., Reining, F., Sakamoto, M., Sookdeo, A., Talamo, S., 2020. The Intcal20 northern hemisphere radiocarbon age calibration curve (0–55 CAL kBP). *Radiocarbon* 62 (4), 725–757. <https://doi.org/10.1017/RDC.2020.41>.
- Ren, Z., 1995. Local Chronicles of Hangzhou Municipality. Chinese Publication House, Beijing, pp. 476. (in Chinese).
- Shi, C., Mo, D., Li, C., Liu, B., Mao, L., Li, M., 2011. The relationship between environmental evolution and human activities in Liangzhu Sites Group, Zhejiang Province, China. *Earth Sci. Front.* 18 (13), 347–356 (in Chinese with English abstract).
- Shu, J., Wang, W., Jiang, L., Takahara, H., 2010. Early Neolithic vegetation history, fire regime and human activity at Kuhuqiao, lower Yangtze River, East China: new and improved insight. *Quat. Int.* 227 (1), 10–21. <https://doi.org/10.1016/j.quaint.2010.04.010>.
- Stanley, D.J., Warne, A.G., 1994. Worldwide initiation of holocene marine deltas by deceleration of sea-level rise. *Science* 265 (5169), 228–231. <https://doi.org/10.1126/science.265.5169.228>.
- Stanley, D.J., Warne, A.G., 1997. Holocene Sea-level change and early human utilization of deltas. *GSA Today* 7 (12), 1–7.
- Stanley, D.J., Chen, Z., Song, J., 1999. Inundation, sea-level rise and transition from Neolithic to Bronze Age cultures, Yangtze Delta, China. *Geoarchaeology* 14 (1), 15–26. [https://doi.org/10.1002/\(SICI\)1520-6548\(199901\)14:1<15::AID-GEA2>3.0.CO;2-N](https://doi.org/10.1002/(SICI)1520-6548(199901)14:1<15::AID-GEA2>3.0.CO;2-N).
- Sun, S., Wu, Y., 1987. Formation and evolution of Taihu Lake and modern sedimentation. *Sci. China Ser. B* (12), 1329–1339 (in Chinese).
- Sun, Q., Liu, Y., Wünnemann, B., Peng, Y., Jiang, X., Deng, L., Chen, J., Li, M., Chen, Z., 2019. Climate as a factor for Neolithic cultural collapses approximately 4000 years BP in China. *Earth Sci. Rev.* 197, 102915. <https://doi.org/10.1016/j.earscirev.2019.102915>.
- Ta, T.K.O., Nguyen, V.L., Tateishi, M., Kobayashi, I., Tanabe, S., Saito, Y., 2002. Holocene delta evolution and sediment discharge of the Mekong River, southern Vietnam. *Quat. Sci. Rev.* 21 (16), 1807–1819. [https://doi.org/10.1016/S0277-3791\(02\)00007-0](https://doi.org/10.1016/S0277-3791(02)00007-0).
- Van Rooij, D., Blamart, D., Richter, T., Wheeler, A., Kozachenko, M., Henriet, J.P., 2006. Quaternary sediment dynamics in the Belgica mound province, Porcupine Seabight: ice-rafting events and contour current processes. *Int. J. Earth Sci.* 96 (1), 121–140. <https://doi.org/10.1007/s00531-006-0086-6>.
- Wang, B., 2019a. The Comprehensive Research of Majiabang Culture. (Dr.), Shanghai University (In Chinese with English abstract).
- Wang, N., 2019b. A water conservancy system outside the Liangzhu Ancient City. In: A Comprehensive Study of Liangzhu Ancient City. Cultural Relics Press, Beijing, pp. 270–284 (in Chinese).
- Wang, Y., Cheng, H., Edwards, R.L., He, Y., Kong, X., An, Z., Wu, J., Kelly, M.J., Dykoski, C.A., Li, X., 2005. The Holocene Asian Monsoon: Links to solar changes and North Atlantic climate. *Science* 308 (5723), 854–857. <https://doi.org/10.1126/science.1106296>.
- Wang, W., Ding, J., Shu, J., Chen, W., 2010. Exploration of early rice farming in China. *Quat. Int.* 227 (1), 22–28. <https://doi.org/10.1016/j.quaint.2010.06.007>.
- Wang, Z., Zhuang, C., Saito, Y., Chen, J., Zhan, Q., Wang, X., 2012. Early mid-Holocene Sea-level change and coastal environmental response on the southern Yangtze delta plain, China: implications for the rise of Neolithic culture. *Quat. Sci. Rev.* 35, 51–62. <https://doi.org/10.1016/j.quascirev.2012.01.005>.
- Wang, Z., Zhan, Q., Long, H., Saito, Y., Gao, X., Wu, X., Li, L., Zhao, Y., 2013. Early to mid-Holocene rapid sea-level rise and coastal response on the southern Yangtze delta plain, China. *J. Quat. Sci.* 28 (7), 659–672. <https://doi.org/10.1002/jqs.2662>.
- Wang, X., Mo, D., Li, C., Yu, S., Xue, B., Liu, B., Wang, H., Shi, C., 2017. Environmental changes and human activities at a fortified site of the Liangzhu culture in eastern China: evidence from pollen and charcoal records. *Quat. Int.* 438, 189–197. <https://doi.org/10.1016/j.quaint.2017.05.001>.
- Wang, Z., Ryves, D.B., Lei, S., Nian, X., Lv, Y., Tang, L., Wang, L., Wang, J., Chen, J., 2018. Middle Holocene marine flooding and human response in the South Yangtze coastal plain, East China. *Quat. Sci. Rev.* 187, 80–93. <https://doi.org/10.1016/j.quascirev.2018.03.001>.
- Wang, S., Ge, J., Kilbourne, K.H., Wang, Z., 2020. Numerical simulation of mid-Holocene tidal regime and storm-tide inundation in the South Yangtze coastal plain, East China. *Mar. Geol.* 423, 106134. <https://doi.org/10.1016/j.margeo.2020.106134>.
- Wenke, R.J., 1991. The Evolution of early Egyptian civilization: issues and evidence. *J. World Prehist.* 5 (3), 279–329. <https://doi.org/10.2307/25800600>.
- Xiong, H., Zong, Y., Qian, P., Huang, G., Fu, S., 2018. Holocene Sea-level history of the northern coast of South China Sea. *Quat. Sci. Rev.* 194, 12–26. <https://doi.org/10.1016/j.quascirev.2018.06.022>.
- Xiong, H., Zong, Y., Li, T., Long, T., Huang, G., Fu, S., 2020. Coastal GIA processes revealed by the early to middle Holocene Sea-level history of East China. *Quat. Sci. Rev.* 233, 106249. <https://doi.org/10.1016/j.quascirev.2020.106249>.
- Yang, T., Zhang, J., Shi, W., 2002. The characteristics of tidal current distribution in Zhipu section of the Hangzhou Bay. *Donghai Mar. Sci.* 20 (4), 1–7 (in Chinese with English abstract).

- Yao, X., 2016. Application of XRF Core Scanning Technology in Holocene Sea Level Change Reconstruction in Ningshao Plain (Master). Nanjing Normal University, Nanjing, China (in Chinese with English abstract).
- Ye, W., Cheng, L., Zhu, L., Li, F., Wang, T., Jin, L., 2015. Grain-size characteristics and evolution of sedimentary environment in Beihuqiao drilling in Zhejiang China. *J. Zhejiang Norm. Univ. (Nat. Sci.)* 38 (3), 255–261. <https://doi.org/10.16218/j.issn.1001-5051.2015.03.003> (in Chinese with English abstract).
- Ye, W., Chen, Q., Zhu, L., Li, F., Wang, T., Cheng, L., Zhang, Y., 2017. Early middle Holocene climate oscillations recorded in the Beihuqiao Core, Yuhang, Zhejiang Province, China. *J. Paleolimnol.* 59, 263–278. <https://doi.org/10.1007/s10933-017-9959-x>.
- Zhang, Y., 2017. Environmental and Vegetation History Variabilities Archived by Pollen-Spore of the Drill Core Beihuqiao2 in Hangjiahu Plain during the Mid-Late Holocene, China (Master). Zhejiang Normal University (in Chinese with English abstract).
- Zhang, Q., Jiang, T., Shi, Y., Lorenz, K., Liu, C., Martin, M., 2004. Paleo-environmental changes in the Yangtze Delta during past 8000 years. *J. Geogr. Sci.* 14 (1), 105–112. <https://doi.org/10.1007/BF02873097>.
- Zhang, Q., Zhu, C., Liu, C., Jiang, T., 2005. Environmental change and its impacts on human settlement in the Yangtze Delta, P.R. China. *Catena* 60 (3), 267–277. <https://doi.org/10.1016/j.catena.2004.12.001>.
- Zhang, X., Lin, C., Dalrymple, R.W., Gao, S., Li, Y., 2014. Facies architecture and depositional model of a macrotidal incised-valley succession (Qiantang River estuary, eastern China), and differences from other macrotidal systems. *GSA Bull.* 126 (3/4), 499–522. <https://doi.org/10.1130/B30835.1>.
- Zhang, Y., Ye, W., Ma, C., Li, Y., Zhu, L., 2020. Middle to late Holocene changes in climate, hydrology, vegetation and culture on the Hangjiahu Plain, Southeast China. *J. Paleolimnol.* 64, 211–223. <https://doi.org/10.1007/s10933-020-00132-2>.
- Zhejiang Provincial Institute of Cultural Relics, Archaeology Xiaoshan Museum, 2004. *Kua Hu Qiao*. Cultural Relics Publishing House, Beijing, pp. 379. (in Chinese with English abstract).
- Zheng, Y., Sun, G., Qin, L., Li, C., Wu, X., Chen, X., 2009. Rice fields and modes of rice cultivation between 5000 and 2500 BC in East China. *J. Archaeol. Sci.* 36 (12), 2609–2616. <https://doi.org/10.1016/j.jas.2009.09.026>.
- Zheng, H., Zhou, Y., Yang, Q., Hu, Z., Ling, G., Zhang, J., Gu, C., Wang, Y., Cao, Y., Huang, X., Cheng, Y., Zhang, X., Wu, W., 2018. Spatial and temporal distribution of Neolithic sites in coastal China: sea level changes, geomorphic evolution and human adaption. *Sci. China Earth Sci.* 61 (2), 123–133. <https://doi.org/10.1007/s11430-017-9121-y>.
- Zhu, C., Song, J., You, K., Hang, H., 1996. Cultural interruptions of the Maqiao Site in Shanghai. *Chin. Sci. Bull.* 41 (2), 148–152 (in Chinese).
- Zong, Y., 2004. Mid-Holocene Sea-level highstand along the Southeast Coast of China. *Quat. Int.* 117 (1), 55–67. [https://doi.org/10.1016/S1040-6182\(03\)00116-2](https://doi.org/10.1016/S1040-6182(03)00116-2).
- Zong, Y., Chen, Z., Innes, J., Chen, C., Wang, Z., Wang, H., 2007. Fire and flood management of coastal swamp enabled first rice paddy cultivation in East China. *Nature* 449 (7161), 459–462. <https://doi.org/10.1038/nature06135>.
- Zong, Y., Wang, Z., Innes, J., Chen, Z., 2012. Holocene environmental change and Neolithic rice agriculture in the lower Yangtze region of China: a review. *The Holocene* 22 (6), 623–635. <https://doi.org/10.1177/0959683611409775>.
- Zong, Y., Zheng, Z., Huang, K., Sun, Y., Wang, N., Tang, M., Huang, G., 2013. Changes in sea level, water salinity and wetland habitat linked to the late agricultural development in the Pearl River delta plain of China. *Quat. Sci. Rev.* 70, 145–157. <https://doi.org/10.1016/j.quascirev.2013.03.020>.